Asian Journal of Research and Reviews in Physics

1(3): 1-17, 2018; Article no.AJR2P.43984

Boron-doped TiO_2 (B-TiO_2) Thin Films Grown Using Sol-Gel Spin Coating Method

D. O. Samson[1,2*] and A. D. A. Buba[1]

[1]Department of Physics, University of Abuja, P.M.B 117, Abuja, Nigeria.
[2]School of Physics, Universiti Sains Malaysia, 11800 USM, Gelugor, Penang, Malaysia.

Authors' contributions

This work was carried out in collaboration between both authors. Author DOS designed the study, performed the statistical analysis, wrote the protocol and wrote the first draft of the manuscript. Authors DOS and ADAB managed the analyses of the study. Author DOS managed the literature searches. Both authors read and approved the final manuscript.

Article Information

DOI: 10.9734/AJR2P/2018/v1i324619
Editor(s):
(1) Dr. Huseyin Cavus, Professor, Department of Physics, Canakkale Onsekiz Mart University, Turkey.
Reviewers:
(1) Aruna P. Maharolkar, Marathwada Institute of Technology, India.
(2) R. Gowrishankar, Sri Sathya Sai Institute of Higher Learning, India.
(3) Ikhioya, I. Lucky, University of Nigeria, Nigeria.
(4) En-Chih Chang, I-Shou University, Taiwan.
Complete Peer review History: http://www.sciencedomain.org/review-history/26664

Original Research Article

Received 20 July 2018
Accepted 04 October 2018
Published 15 October 2018

ABSTRACT

In this study, the effect of modifying boron doping concentration on the optical properties, electrical properties and microstructural images of TiO_2 thin films was investigated by the sol-gel technique by grinding TiO_2 powder with a boron compound at a wavelength range of 250 nm to 850 nm. The SEM micro-images revealed the homogenous, continuous and nanocrystalline surface morphology: 10% is the tolerable amount of boron doping concentration into the TiO_2 for achieving sphere-like nanostructures materials with low agglomeration. The XRD spectra of the B-TiO_2 films showed anatase peaks of greater intensities when compared to the pure TiO_2 film. All the films illustrate extinction coefficient in the visible region of solar spectra corresponding to the low absorption, and absorption peaks established in the ultraviolet region near 330nm with the optical transmittance varied from over 52 - 96% in the UV-Vis wavelength range. Diffuse reflectance absorption spectra analysis indicated that the incorporation of B into TiO_2 material results in a substantial red shift and the absorption extends significantly into the visible range. The optical band gap energy values of the thin films were found to be 3.38, 3.35, 3.28, 3.26, and 3.36eV. This showed a low probability of

**Corresponding author: E-mail: damilola.samson@uniabuja.edu.ng;*

raising the electron across the mobility gap with the photon energy in the visible region. The refractive index values varied between 1.891 and 1.922 depending on the percentage content of boron. Moreover, the imaginary part of the dielectric constant increase slowly, whereas the real part increases sharply and the optical conductivity was found to increase with the increase in boron addition.

Keywords: B-TiO_2; Sol-gel; optical properties; refractive index; dielectric constant; thin films.

1. INTRODUCTION

Metal oxide semiconductor materials play a vital role in various areas of science and engineering. Titanium (IV) oxide (TiO_2) films has attracted lots of significance attention, among many semiconductor nanoparticles. This is attributed to its practical applications, which extends from common products to the advanced technological applications such as photovoltaics, solar cells, photocatalysis, antireflective films coatings, optical coatings, electrochromic display devices, bio-sensing, hydrogen gas production, bactericidal action, and so on [1-6]. It has been regarded as a fantabulous semiconductor photocatalyst because of its high performance, abundance, low toxicity, low cost, outstanding thermal and chemical stability, and photo-induced strong oxidation activity properties [7-8]. Anatase, brookite, rutile and amorphous are the four polymorphic that constitutes crystal structures of titania. TiO_2 is a major actor in the emerging field of oxide electronics and is regarded as the most efficient and environmentally friendly photocatalyst but its application suffers some drawbacks in visible light: ultraviolet activation requirements due to its large band gap energy (3.2eV for anatase and 3.06eV for rutile) and low degradation kinetic [9]. It is also well known that TiO_2 have high rate recombination between the excited electron and positive hole. Recombination of electron-hole pairs has been described as the main factor limiting photocatalytic reactions. Some of the photogenerated pairs achieve charge separation and diffuse to the TiO_2 surface, reacting with air or water and generate OH radicals, O anions, which attack the organic compounds adsorbed on the TiO_2 surface causing their removal by transforming into CO_2 and H_2O. Different strategies have been employed in investigating and improving the optical, electrical and photocatalytic characteristics performances of TiO_2, which have necessitated the doping of the material to extend the optical absorption within the visible region and reduce the electrons or holes recombination rate [4,10]. These strategies include the generation of structured mesoporous materials, decreasing band gap, increasing surface area, extending the light absorption range by incorporating foreign elements, metals or non-metals into the TiO_2 matrix, reducing particle size, and creating a double phase structure containing anatase and rutile [11]. Series of elements have been doped into various semiconductor nanoparticles and establish a great success in ameliorating their properties over the pure nanoparticles. Doping TiO_2 implies the interstitial or substitutional insertion of other atoms, cations or anions in the TiO_2 crystalline cell [12]. Different dopant (impurity) elements, such as metals, metalloids, and non-metals have been applied for modulating the properties of nanoparticles. Modification of TiO_2 by impurities doping can produce a high Schottky barrier that facilitates electron capture, which may produce longer electron-hole pair separation lifetime and reduce the recombination of electron-hole pair separation [13]. Due to the high thermal stability and low carrier recombination centres of non-metals doped TiO_2 nanostructures, there has been an explosion of concern in TiO_2 doping with non-metal ions: N, C, S, F, P, I, and B, that has been explored to boost and enhance separation of photogenerated charges in TiO_2 under ultraviolet or visible light [4,11,14]. The use of these anionic dopants leads to band gap narrowing or formation of localised mid-band gap states, which effectively extends the absorption threshold of titania into the visible region and causing physical and chemical changes in the particles [15]. Doping TiO_2 with B can extend the spectral response of TiO_2 to visible region and thus can improve its visible light photocatalytic activity, and promotes photogenerated electron-hole separation [4,16-17]. When boron is doped into the TiO_2 lattice, boron atoms can occupy two different positions (Interstitial and substitutional) by filling up the oxygen vacancies [18]. The stability of the doped TiO_2 is far better when boron occupies an interstitial position within the TiO_2 lattice compared to the substitutional boron, which appears to be metastable and decompose into boron oxide [19]. Various forms of techniques have been used to prepare B-TiO_2 thin films: Thermal evaporation, anodic oxidation, chemical vapour deposition, pulsed laser

deposition, electron beam evaporation, spray pyrolysis, hydrothermal, sol-gel techniques, etc. [5,20-23]. Amongst this technique the sol-gel process, as a very promising method, has gained particular attention due to its simplicity, inexpensiveness, non-vacuum, ability to produce thin and homogeneous films on large substrate area and low temperature technique for synthesising films using organic and inorganic precursors. This process offers many benefits like perfect control of the stoichiometry of precursor solutions, ease of compositional modifications, customizable microstructure, ease of introducing various functional groups, requiring relatively low annealing temperatures and the possibility of coating over large area substrates [21,24]. The main objective of this study, therefore, is to establish the suitable synthesis conditions of undoped TiO_2 and B-TiO_2 thin films on the glass substrate by sol-gel technique to obtain high quality transparent thin films for optoelectronic and optical applications in the wavelength range of 250 nm to 850 nm.

2. EXPERIMENTAL DETAILS

2.1 Materials

Titanium tetrachloride [$TiCl_4$] (Merck), Boric acid [H_3BO_3] (BDH) (≥ 99.9% purity, Aldrich), Acetylacetone [$CH_3COCH_2COCH_3$] (BDH) with ≥ 99.9% purity (Aldrich), Ethanol (BDH) (99.7% purity, Aldrich), Cleaning solution [sodium lauryl] and Ammonia solution [NH_4OH] (*ca.* 33%wt NH, Merck) were purchased from Quality Control and Testing Laboratories Ltd. Distilled water was prepared in our laboratory with pH 5.8. All other reagents and solvents used for this study were of analytical grade and do not require any further purification.

2.2 Synthesis of TiO_2 and B Doped TiO_2 Nanoparticles

Boron doped titanium dioxide (B-TiO_2) and pure TiO_2 thin films were synthesised by the sol-gel spin coating technique onto a glass substrate in this work using $TiCl_4$ and boric acid as source materials. The optical glass substrates were degreased and washed ultrasonically in a cleaning solution containing sodium lauryl detergent and subsequently rinsed with distilled water and then with propanol, dried under compressed air until observed fully dried and kept in a dry petri dish. The percentage doping concentration of B-TiO_2 thin films was obtained by adding suitable proportions (B / [B+Ti] = 5 - 20%) of $TiCl_4$ in the starting solutions. 10 ml of distilled water was added to the 25 ml of $TiCl_4$ and moderately stirred at room temperature for 1 hour until a clear and uniform solution was obtained. The resulting solution was kept in an air tight beaker for 24 hours at room temperature, to improve the homogeneity of the prepared mixture and adapted for deposition. Then the complex was hydrolysed by adding an aqueous solution of ammonia drop-wise over a period of 30 minutes via an adjustable pipette until the pH value of 10 was obtained, to precipitate peroxotitanium hydrate. The resultant peroxotitanium hydrate precipitate was washed several times with distilled water, rinsed with absolute ethanol to remove chloride ion and ammonia and dried in a vacuum oven at 60^{o}C for 1 hour. Then the sol was prepared by adding 0.38 g of peroxotitanium hydrate into 11ml of distilled water for hydrolysis polycondensation reaction and mixed thoroughly with a magnetic stirrer until yellow and transparent peroxotitanium acid solution was formed. Homogeneous light yellow and translucent peroxo-modified anatase anhydrate solution obtained by heating the solution at 80°C for 8 hours with consistent stirring in order to crystallize anatase. Five coatings of B-TiO_2 at different boron doping concentration of 0, 5, 10, 15 and 20% were prepared on the ultrasonically cleaned glass substrates by spin-coating process at a speed of 3000rpm. The B-TiO_2 thin films were synthesized by dissolving the peroxo-modified anatase anhydrate in distilled water. The resulting solution was spin-coated on the prepared glass substrate at 3000 rpm for 30 seconds in an air, leading to the procured of undoped TiO_2 thin films and annealed at 500°C for 45 minutes and which were homogeneous, transparent, and highly adherent across the whole length of the glass substrates. The boron doped TiO_2 thin films were obtained by dissolving the peroxo-modified anhydrate and boric acid in distilled water with concentration of boric acid at 0.05mol/dm^3 to obtain 5% B concentration. The solution was spin-coated on the glass substrate at 3000rpm for 30 seconds and annealed at 500^{o}C for 45 minutes. This process was repeated with a concentration of boric acid at 0.10, 0.15 and 0.20mol/dm^3 to obtain 10, 15 and 20% doping concentration of boron.

2.3 Microstructural Characterization

The morphology characterisation of the material powders was analysed with an EVO I MA10 scanning electron microscope (SEM) at an accelerating voltage of 20kV. The samples were

mounted on carbon tape and sputter-coated with gold.

2.4 X-ray Diffraction (XRD) Characterization

The XRD patterns of the thin films were measured using an XRD system (D8 Advance Diffractometer, X'Pert' Powder PANALYTICAL Bruker) with a monochromatic Cu- K_α ($\lambda = 1.5406$Å) radiation, operating voltage of 42kV and current of 40mA. The system was operated in a scan rate of 0.040° increments with a measuring time of 3.17s per step in the range of 2θ = 20° - 80°. The lattice parameter 'a' and 'c' values of B-TiO_2 compared to the pure TiO_2 with respect to different doping concentration were determined using the Bragg's relations (1) and the interplanar spacing (d) was evaluated using the formula for a tetragonal structure (2) [25]:

$$2d \sin\theta = \lambda \quad (1)$$

$$\frac{1}{d^2} = \frac{4}{3}\left[\frac{h^2 + hk + k^2}{a^2}\right] + \frac{l^2}{c^2} \quad (2)$$

$$a = \sqrt{\frac{1}{3}}c \quad , \quad c = \frac{\lambda}{\sin\theta} \quad (3)$$

Where, λ is the wavelength of the Cu-K_α X-rays and θ is the diffraction angle at which the maximum intensity was observed.

2.5 Optical Characterization

UV-Vis spectrophotometer is a valuable technique that can be applied to examine the electronic structure and band gap energies of semiconductors. The optical properties of the synthesised B-TiO_2 thin films deposited on glass substrates were analysed by using Axiom Medicals UV-Vis 752 spectrophotometer equipped with an integrating sphere for diffuse reflectance. Optical transmission measurements were carried out within a wavelength range of 250nm to 850nm, although most cases are performed within the range of 380nm to 850nm. The spectrophotometer was set with a slit width of 1nm and hence no slit correction was required. As the light is transmitted, the sample disrupts the path of the beam, a portion of light was absorbed, a fraction was reflected, or scattered from small particles suspended in the sample, and the rest was transmitted through the sample. The transmission measurements were determined in different parts of the film, scanning the entire sample, and good reproducibility of the respective samples was generally observed. The absorbance of the sample was examined using the Beer-Lambert law, which describes the spectral transmission of the light beam through an absorbing medium and is expressed as:

$$A = -\log_{10}\left(\frac{I_t}{I_i}\right) = -\log_{10} T \quad (0 < T < 1) \quad (4)$$

$$T = \frac{I_t}{I_i} \quad (5)$$

$$\%T = \left(\frac{I_t}{I_i}\right) \times 100 \quad (6)$$

Where, I_t is the intensity of the transmitted light, I_i is the intensity of the incident light at a given wavelength, A is the measured absorbance, and T is the measured transmittance. From the Beer-Lambert relations, if all the light passes through a medium without any absorption, then absorbance is zero, and percent transmittance is 100%, but if all the light is absorbed, then percent transmittance is zero, and absorption is infinite. The reflectance (R) was computed from the transmittance and absorbance using the expression in equation (7):

$$R = 1 - T - A \quad (7)$$

2.5.1 Absorption coefficient (α)

The absorption coefficient (α) determines how far into a material light of a particular wavelength can penetrate before it is absorbed. The absorption coefficient (α) of B-TiO_2 thin films was determined using the following relation [26]:

$$\alpha = \frac{2.303A}{t} \quad (8)$$

Where, t is the thin film thickness, and A is the absorbance.

2.5.2 Calculation of extinction coefficient (k)

The extinction coefficient (*k*) is a measure of the fraction of light lost due to scattering and absorption per unit distance of the penetration medium. It describes the attenuation of light in a medium and increase of *k* with the increase of $h\nu$ indicates the probability of raising the electron transfers across the mobility gap with photon energy. Therefore, the higher values of *k* are the

representation of greater attenuation of light in a thin films and also the higher probability of raising the electron transfer across the mobility gap with the photon energy. The extinction coefficient of the films can be calculated from the values of α and λ using the relation [27]:

$$k = \frac{\alpha\lambda}{4\pi} \tag{9}$$

Where, λ is the wavelength, and α is the absorption coefficient.

2.5.3 Band gap energy (E_g)

It is well known that in the sol-gel process, the organic products from the precursors would also influence the crystallinity as well as the optical properties of the thin films. The optical band gap energy (E_g) is the energy needed to move a valence electron into conduction band. E_g of TiO_2 thin films was obtained in the extinction of coefficient (k) [28,29]:

$$C(E - E_g) = (\alpha h\nu)^{n/2} = \left[\left(\frac{4\pi k}{\lambda}\right) h\nu\right]^{n/2} \tag{10}$$

Where, h is the plank's constant, and ν is the frequency of the incident photons, $h\nu$ is the energy of the photon energy, λ is the wavelength of the absorption edges in the UV-Vis spectrum, C is a constant depending on the transition probability and n is a number that determined the type of the optical transition of the gap materials ($n = 1$ for direct gap materials and $n = 2$ for an indirect gap materials). Since TiO_2 is direct gap material therefore the above relation becomes:

$$C(E - E_g) = \left[\left(\frac{4\pi k}{\lambda}\right) h\nu\right]^{1/2} \tag{11}$$

The value of the optical band gap energy (E_g) is computed by extrapolating the linear plot of $(\alpha h\nu)^2$ against photon energy $(h\nu)$ of the films known as Tauc's plot for the direct optical band gap materials and have been drawn for thin films deposited with different concentration as illustrated in Fig. 6 [30], this means that the mode of transition in these films is of a direct nature.

2.5.4 Refractive index

The refractive index of the thin films obtained from the transmission spectra using the expression in equation (12) and considered highest transmission (T_{max}) at wavelength 850 nm and lowest transmission (T_{min}) at wavelength 380nm.

$$n = \sqrt{\left\{\left(\frac{n_a^2 + n_g^2}{2} + 2n_a n_g T_o\right) + \left[\left(\frac{n_a^2 + n_g^2}{2} + 2n_a n_g T_o\right)^2 - n_a^2 n_g^2\right]^{1/2}\right\}} \tag{12}$$

$$T_o = \frac{T_{max} - T_{min}}{T_{max} \times T_{min}} \tag{13}$$

Where, T_o is the total transmittance, n_a and n_g are the refractive index of air and glass respectively.

2.6 Dielectric Properties

The real part of the dielectric constants reveals how much it will reduce the speed of light in the material, whereas the imaginary part reveals how a dielectric material absorbs energy from an electric field due to dipole motion. The expression for the real and imaginary parts of the dielectric constant has the following form [25]:

$$\varepsilon_r = n^2 - k^2 \tag{14}$$

$$\varepsilon_{im} = 2nk \tag{15}$$

Where, ε_r and ε_{im} are the real and imaginary parts of the dielectric constant.

2.7 Optical Conductivity

A QUADPRO-301-6 four-point probe system was used to measure the sheet resistance and the resistivity of the deposited thin films after which the optical conductivity was determined from the resistivity. The current value was gradually increased from 0 to 100 μA with a 10 μA step. A source meter was used as the current source applied to the outer probes. The voltage on the inner probes was determined by a VA multimeter. The sheet resistance (R_s) was expressed as:

$$R_s = 4.53 \times \frac{V}{I} \tag{16}$$

Where, V is the voltage measured on the internal probes and I is the current applied to the external probes. The optical conductivity was computed from the relation:

$$\rho = R_s \times t_c \tag{17}$$

$$\sigma = \frac{knc}{\lambda} \tag{18}$$

Where, t_c is the thickness of the conducting layer, ρ is the resistivity, σ is the optical conductivity, c is the speed of light, n is the refractive index, and k is the extinction coefficient.

3. RESULTS AND DISCUSSION

3.1 Surface Morphology

The morphological characteristics of the pure TiO_2 and B-TiO_2 thin film deposited on glass substrate were observed at various boron percentage doping concentrations as illustrated in Fig. 1(a - e).

It is clearly indicated from the above figures that, all the thin films were well attached to the substrates. SEM observations reassert the existence of morphology discrepancies between the boron doped titania. The SEM images of pure TiO_2 (0%) particles showed self-assembled and sphere-like nanostructures (Fig. 1a). B doped TiO_2 at 5% doping concentration revealed spherical shaped particles which show titania constituted of large well-aggregate particles

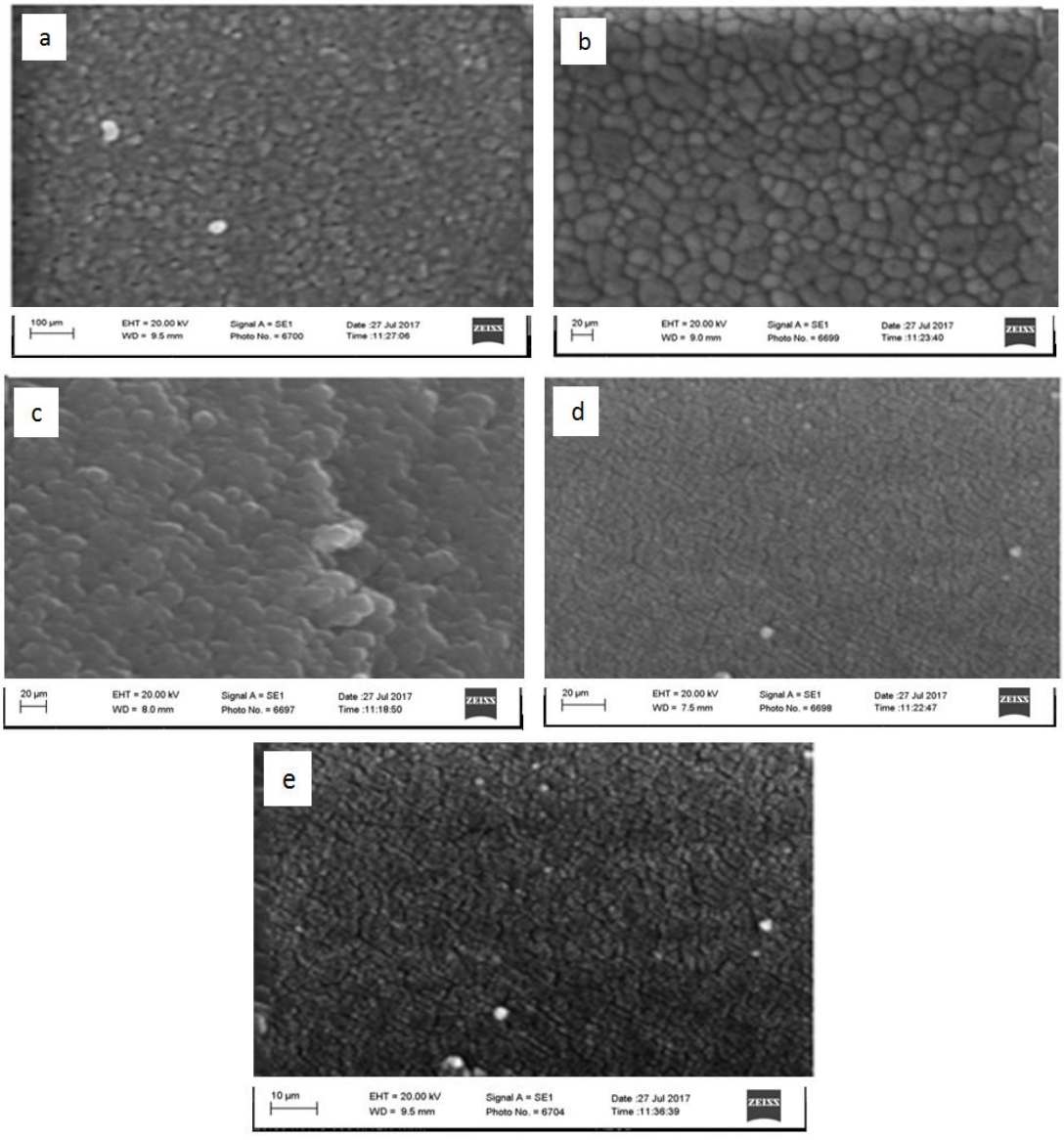

Fig. 1. SEM images of (a) pure TiO_2 (0%); (b) B doped TiO_2 (5%); (c) B doped TiO_2 (10%); (d) B doped TiO_2 (15%); and (e) B doped TiO_2 (20%) thin films

with sizes in the range of 500 nm – 290 nm (Fig. 1b), but at 10% boron doping concentration, agglomeration tendency decreased by doping, in which the film structure is in the form of clusters of crystallites of titania (Fig. 1c). However, further increased doping concentration to 15% and 20% resulted in micrometre-sized agglomerations of particles which is similar to the pure TiO_2 microstructure (Fig. 1d,e). The titania micro structure films were obtained from partially reduced TiO_2 where ordered light band assigned to the polycrystalline TiO_2, and bridges between the strips bright spots to oxygen vacancies [31].

3.2 X-ray Diffraction

The XRD crystal structure of pure TiO_2 and B doped TiO_2 phase deposited from the starting solutions having 5, 10, 15, and 20% of (B / [B+Ti]) ratio are presented in Fig. 2, indicating an interstitial doping of the boron element, and the lattice parameters 'a' and 'c' values are shown in Table 1.

Table 1. The lattice parameters 'a' and 'c' values of pure TiO_2 and B-TiO_2 with different doping concentrations

Sample doping concentration	'a' (nm)	'c' (nm)
TiO_2	0.37942	0.95286
5%B	0.37915	0.95139
10%B	0.37968	0.95158
15%B	0.37920	0.95022
20%B	0.37958	0.94957

X-ray diffraction analysis illustrates that the thin films structure composed of an amorphous phase and anatase to rutile phase transformation and that there was no observable structural difference between undoped TiO_2 and B-TiO_2 as indicated in Fig. 2(a-e). The peaks of the pure TiO_2 film depict that the film is nanocrystalline with tetragonal structure and the preferred orientation is along the (101) plane. The width of the (101) plane diffraction peak $(2\theta = 25.50°)$ of anatase phase shows wider, which reveals the formation of fine crystallites in the thin films, due to reduction in the particle size of B-TiO_2 [32]. As the temperature increase, the peak intensity of the anatase phase increases and the width of the (101) plane gradually becomes narrower, as a result of the growth of crystallites and improvement of crystallisation. The intensity of (004), (200), (105), (204), and (116) planes diminishes as the B concentration increases. There is a slight variation in the lattice parameter along the a-axis while the c-axis parameter decreases as the doping concentration of boron increases as shown in Table 1. The decrease in c-axis parameter indicates that boron ion may be present in the interstitials site of anatase phase, which can balance the residual charge of titania nanoparticles, rather than at the substituted site of oxygen ion. This might be caused due to the B_2O_3 phase separation which might be under the XRD detection limit [33]. The interstitial boron is extremely stable at all temperatures, indicating that interstitial boron is the preferred and the most stable site in TiO_2 compared to the previous report [34].

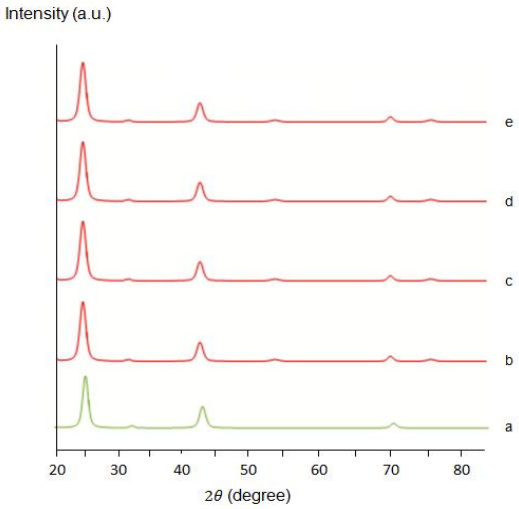

Fig. 2. XRD patterns of pure TiO_2 and B-TiO_2 with different B concentrations: (a) 0%, (b) 5%, (c) 10%, (d) 15%, and (e) 20%

3.3 Optical Properties

3.3.1 Optical transmittance

The optical transmission spectra (%T) of light photons that pass through the undoped TiO_2 and B-TiO_2 {(B / [B+Ti]) = 5, 10, 15, 20%} thin films are illustrated in Fig. 3 in the wavelength range 380nm to 850nm. The figure shows the variation of transmittance with the doping concentration of boron as a function of wavelength.

Fig. 3 indicated that all the thin films deposited have high transmittance values in the range of 90 - 96% within the visible spectra region but with a minimum transmittance of 52% observed for the undoped TiO_2 thin films. The transmittance increases with the increase of B concentration up to 15% concentration and then decreases for (B / [B + Ti]) = 20% doping concentration, but still higher than that of undoped TiO_2 with the increase of annealing temperature and with the number of dipping. This is as a result of the formation stage of anatase phase due to the increase in the grain size. This shows that the values of transmittance are high in the visible and near-infrared region and it is minimum in the ultraviolet region. The films have exhibited higher transmission in the solar spectral range. The increase in transmittance value can be attributed to the decrease in free carrier absorption due to the elevated carrier mobility of the films [35]. Slightly shift of transmittance curves to higher wavelengths is observed for B-TiO_2 thin films in comparison with undoped TiO_2. The overall transmittance behaviour of the undoped TiO_2 and B-TiO_2 thin films indicate uniformity of the thin film thickness and less absorbing nature of the surface.

3.3.2 Optical absorbance

The optical absorption spectra of undoped TiO_2 and B-TiO_2 nanoparticles was estimated using UV-Vis spectroscopy and the spectrum are shown in Fig. 4, in the wavelength range 300nm – 850 nm. The figure illustrates the variation of absorbance with the doping concentration of boron.

From the above figure, it is observed that the optical absorption decreases with the increases doping concentration of boron for the B-TiO_2 thin films. When boron occupies simultaneously both positions within the TiO_2 lattice, the absorbance of ultraviolet light and also the absorbance in the visible range of the spectra increased. These spectra show high absorbance in the wavelength range from about 320 nm – 380 nm (ultraviolet region) and absorption peaks are found in the ultraviolet region near the wavelength 330nm but very low at the visible and infrared regions of solar spectra because of higher transmittance of the thin films in this region. With increasing the numbers of boron concentration there was a red shifting of the absorption peak for up to 1%, which then shifted from higher visible region to lower visible region. The higher concentration of grain boundaries in this film resulted to the broadening of the absorption band edge and consequently shifts the optical band gap energy of TiO_2 in the presence of boron doping, this could be attributed to the decrease of TiO_2 crystal size. The boron doping may also result to the formation of partial Ti^{3+} that can lead to limiting the recombination rate of charge carriers [26]. These films can be used as ultraviolet protected films for optoelectronic devices

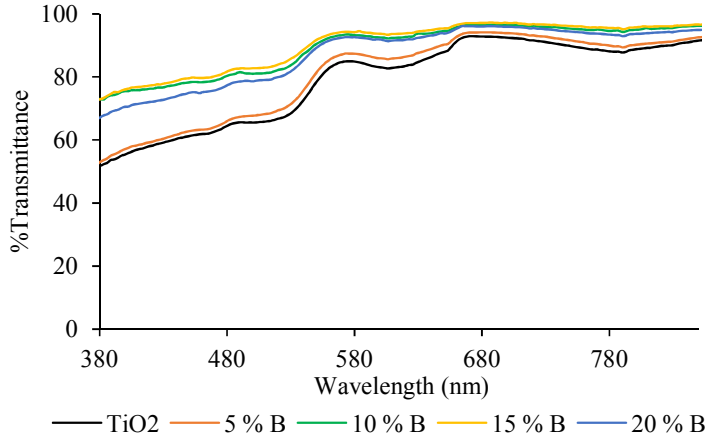

Fig. 3. Optical transmission spectra of undoped TiO_2 and B-TiO_2 thin films deposited at 0, 5, 10, 15 and 20%

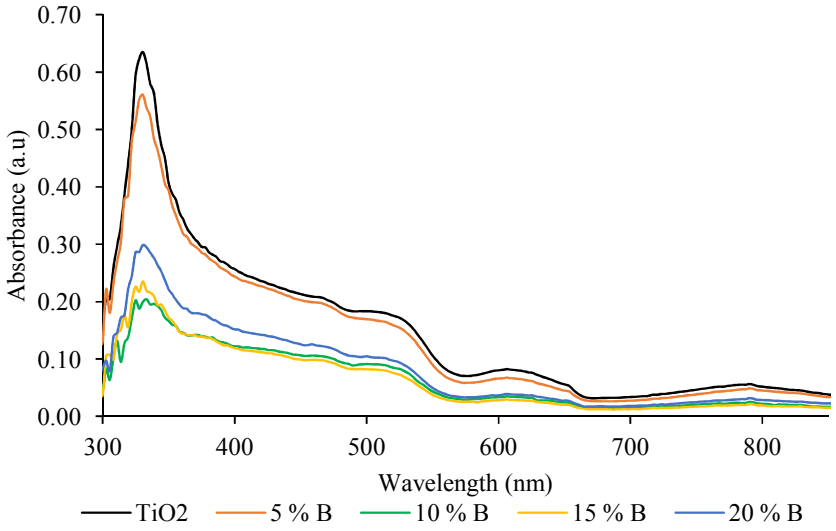

Fig. 4. Absorption spectra of undoped TiO_2 and B-TiO_2 with different B concentration at 0, 5, 10, 15 and 20%

because it has less than 45% transmittance in the ultraviolet region. The absorption edges indicate the transformation from absorption to transmittance regions. The average transmittance of all the thin films in the visible region is approximately 96%. The variations in the transmittance and absorption edge wavelength of titania thin films can be ascribed to the difference in surface morphologies, phase structure, crystallite size, and compositions within the thin films.

3.3.3 Optical reflectance

The extrapolation of the diffuse reflectance absorption spectra versus wavelength curves of the undoped TiO_2 and B-TiO_2 at different B doping concentrations are shown in Fig. 5.

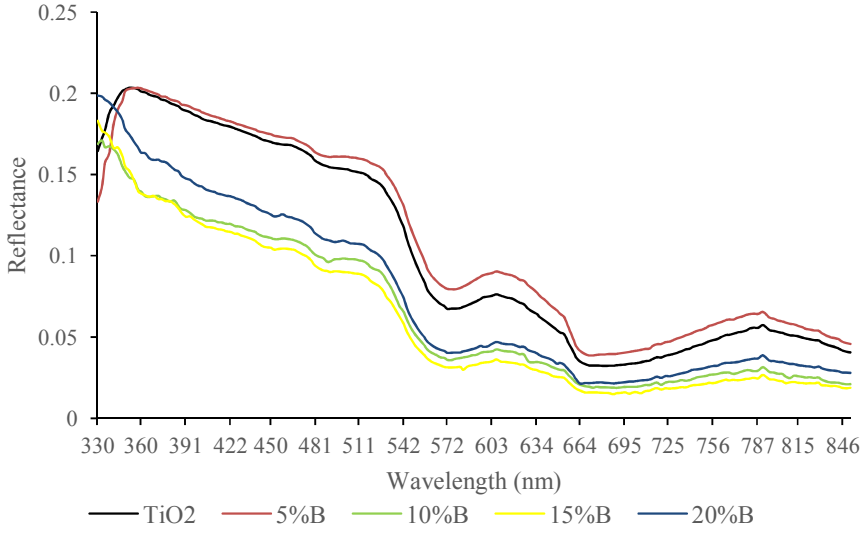

Fig. 5. Diffuse reflectance spectra of pure TiO_2 and B-TiO_2 with various B concentration at 0, 5, 10, 15, and 20%

It is clearly revealed that the incorporation of B into TiO_2 material results in a substantial redshift, and the absorption extends significantly into the visible region, with the (B / [B+Ti]) = 5% indicate large scattering component. The doped films behave like metals in the infrared region, having high reflectance, while in the visible region, it behaves like a dielectrics and is highly transparent. The suppression of the reflection is enhanced accompanying with the increase of doping contents of boron, which displays broadband and high antireflection performance over the solar spectrum.

3.3.4 Optical band gap energy

Optical band gap energy (E_g) of the undoped TiO_2 and B-TiO_2 thin films in the wavelength range 300nm - 850nm, were determined from the Tauc's relation (equation 11) using the extinction coefficient as presented in Fig. 6 (a-e). This plots has two regions: one is high absorption region $(\lambda \geq 330nm)$ and the other is high transmittance region$(\lambda \geq 658nm)$. Both obtained experimental values for the band gap energy are very close to each other for the pure TiO_2 and B-TiO_2.

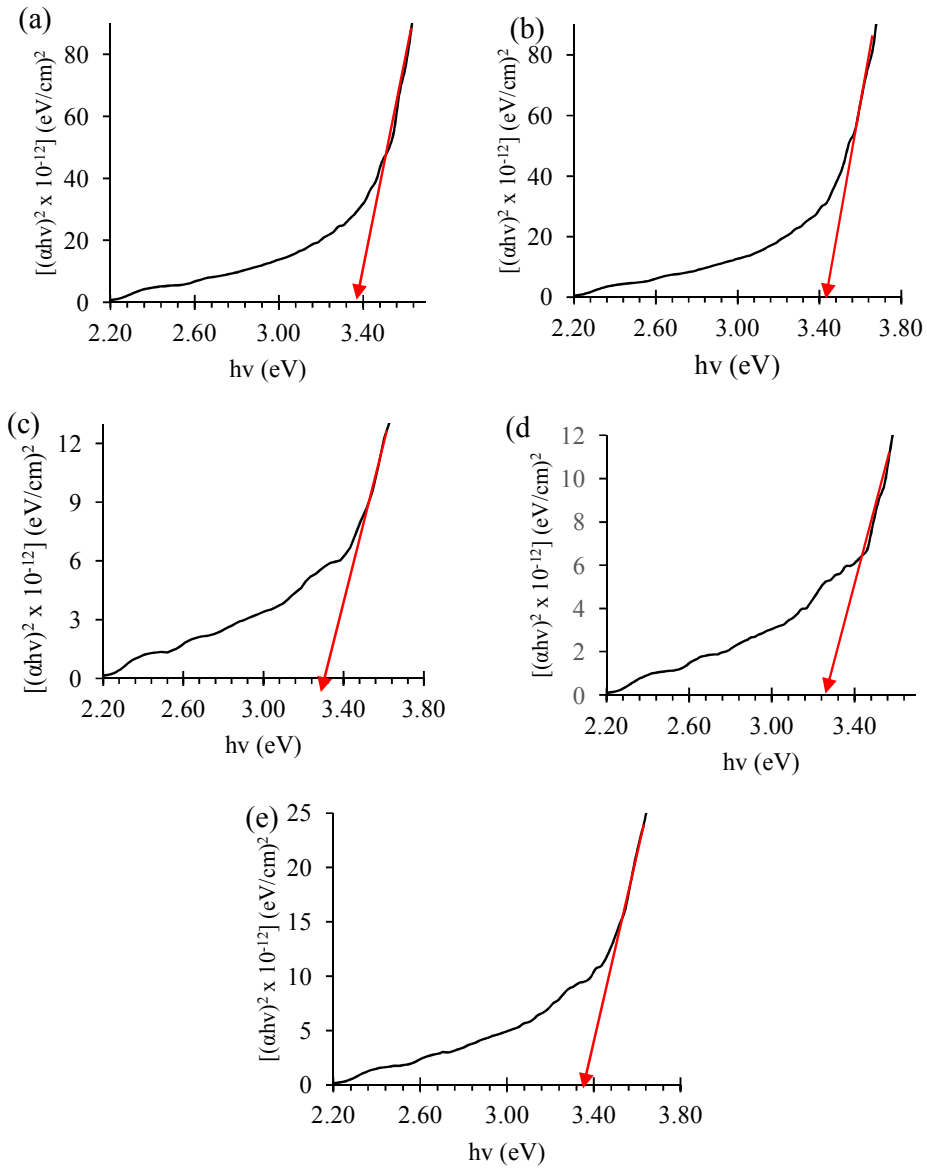

Fig. 6. Band gap energy plots of undoped TiO_2 and B-TiO_2 thin films deposited at (a) 0 (b) 5, (c) 10, (d) 15 and (e) 20%

The extrapolations of the linear portion to the intercept of energy axis at $(\alpha h\nu)^2 \rightarrow 0$ are used to find out the E_g of the undoped TiO_2 and B-TiO_2 thin films. The band gap energy (E_g) values of the thin films is found to be 3.38, 3.35, 3.28, 3.26, and 3.36eV for (B / [B+Ti]) = 0, 5, 10, 15, and 20% boron doping concentration respectively, with the undoped TiO_2 having the highest optical band gap energy of 3.38eV. The decrease in the optical band gap energy is as a result of the increases in boron doping concentration, and then it increases with further increasing the doping percentage, which also induces crystallinity. This implies by adding TiO_2 material into B material, the band gap of B become decrease and ameliorate the minimum energy needed for electron excitation from valence band to conduction band which connote the light with photon energy required to be equal or greater than optical band gap energy absorbed by the semiconductor, the electron will have enough energy to shift from the valence band to the conduction band. The shifting of the anatase peak and the phase change might be due to the doping concentration of the boron to TiO_2, leads to the transformation of the amorphous structure into anatase [22,36]. The obtained results are close to literature data obtained for nanostructured boron doped TiO_2 thin films deposited onto the glass substrate by using sol-gel dip coating method under different deposition conditions [24,36-37]. The variation of optical bandgaps with boron concentrations in TiO_2 thin films are illustrated in Fig. 7.

The band gap energy value decreases from 3.38eV to 3.26eV as boron doping concentration increases (between 0 and 15%) which maybe due to *sp-d* exchange interactions and big crystallite size $(d > 15nm)$ which could be theoretically explained using the second-order perturbation theory [24,38]. This behaviour has been observed and reported by Begum et al. [39] on boron-doped TiO_2 thin films prepared by liquid phase deposition technique. However, the E_g increased to 3.36eV when boron concentration is increased from 15 to 20%. The increase of E_g value at 20% of boron concentration may be attributed to the Burstein-Moss effect [24]. The undoped TiO_2 films exhibit higher optical band gap energy and blue shift as a consequence of exciton confinement due to decreased grain size and increased pore volume. The enhancement of absorbance in the ultraviolet region increases the number of photogenerated electrons-holes to participate in the photocatalytic reaction, which can enhance the photocatalytic activity of TiO_2, whereas the band gap only revealed a slight decrease in energy and the reduction of recombination rates for photoexcited electrons-holes [37]. Thus, the valence electrons require an additional energy to be excited to the higher energy states in the conduction band to conserve linear momentum, due to the slight band gap energy shifted. The obtained band gap energies for the thin films are larger than the band gap energies of anatase and rutile titania, which might be due to the thermal stress in the thin film as a result of the difference in the thermal expansion coefficients between the substrate and the titania films.

3.3.5 Extinction coefficient (k)

The values of extinction coefficient spectra of TiO_2 and B-TiO_2 are shown in Fig. 8 as a function of wavelength.

The dependence of the extinction coefficient on the wavelength for the deposited thin films are indicated in Fig. 8. All the thin films show extinction coefficient (*k*) in the visible region of solar spectra corresponding to the low absorption and absorption peaks are found in the ultraviolet region near the wavelength 330nm. Extinction coefficient gradually increases with the decrease of wavelength as the boron doping concentrations decreases and sharply increase at the fundamental absorption edges where the wavelength threshold corresponds to the band gap of TiO_2 bulk crystal [40]. Moreover, as the wavelength increase, the extinction coefficient decreases, this revealed that the fraction of light lost due to scattering and absorbance decreases. All the B-TiO_2 thin films exhibit low values of *k* since the transmittance values are high.

3.4 Refractive Index

The variations of the refractive index of deposited samples are listed in Table 2 and Fig. 9 gives the graphical representation of the refractive index. The refractive index revealed the direct effect of crystalline structure of the thin films.

Table 2. Average refractive indices of pure TiO_2 and B-TiO_2 thin films at different concentrations

Sample code	Refractive index (n)
TiO_2	1.910
5%B	1.913
10%B	1.922
15%B	1.904
20%B	1.891

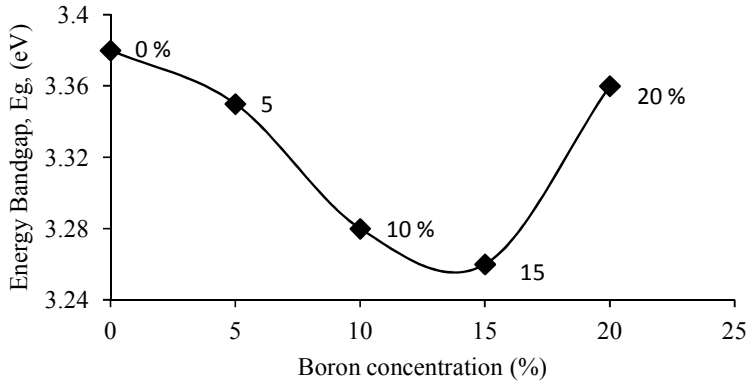

Fig. 7. Variation of optical band gaps energy with boron concentrations in TiO_2 thin films deposited at 0, 5, 10, 15 and 20%

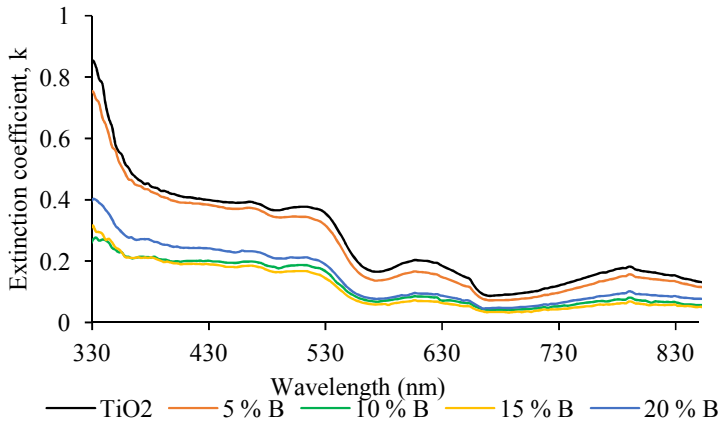

Fig. 8. Variation of extinction coefficient (*k*) as a function of wavelength for pure TiO_2 and B-TiO_2 thin films at different doping concentration

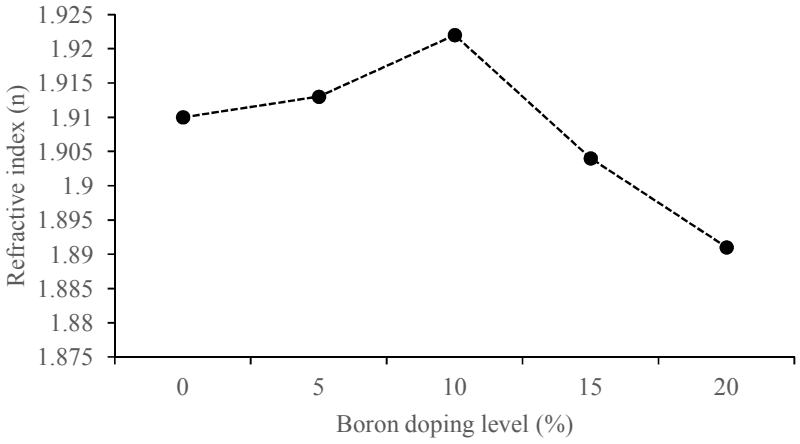

Fig. 9. Variation of refractive indices of pure TiO_2 and B-TiO_2 thin films at 0, 5, 10, 15, and 20% concentrations

From the above figure, the refractive index of the film significantly changes with the deposition parameter. It shows that the refractive index increases with increasing B doping concentrations up to 10% from 1.910 to 1.922. As B doping concentrations increased above (B / [B+Ti]) = 10%, the refractive index of the thin films drastically decreased from 1.922 to 1.891 {(B / [B+Ti]) = 15 and 20%}. This rapid changes in refractive index of the thin films might due to the thermal induced growth of the grains which lead to an increase in the packing density of TiO_2 thin film by boron, because the ion radius of TiO_2 is larger than that of the boron, which leads to the formation of a high ratio of metal-oxygen-metal frame in boron doped titania, resulting in a dense film.

3.5 Dielectric Constant

The real and imaginary parts of the dielectric constant with respect to the boron doping levels are shown in Figs. 10 and 11.

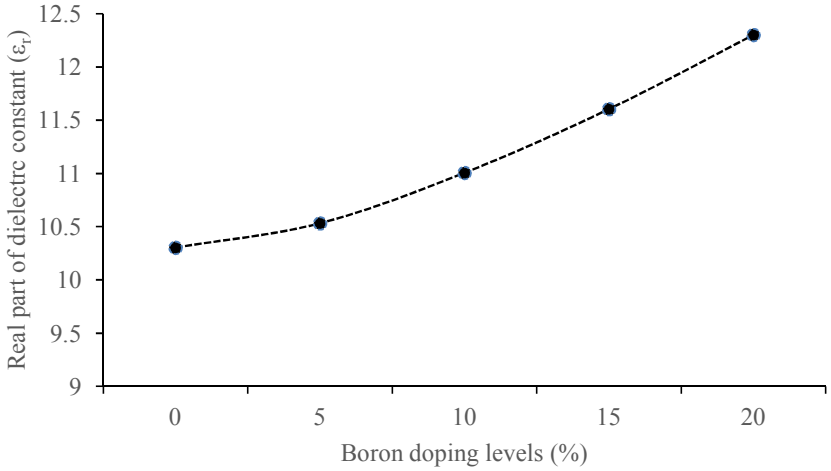

Fig. 10. Variation of real part of dielectric constant of pure TiO_2 and B-TiO_2 thin films at 0, 5, 10, 15, and 20% concentrations

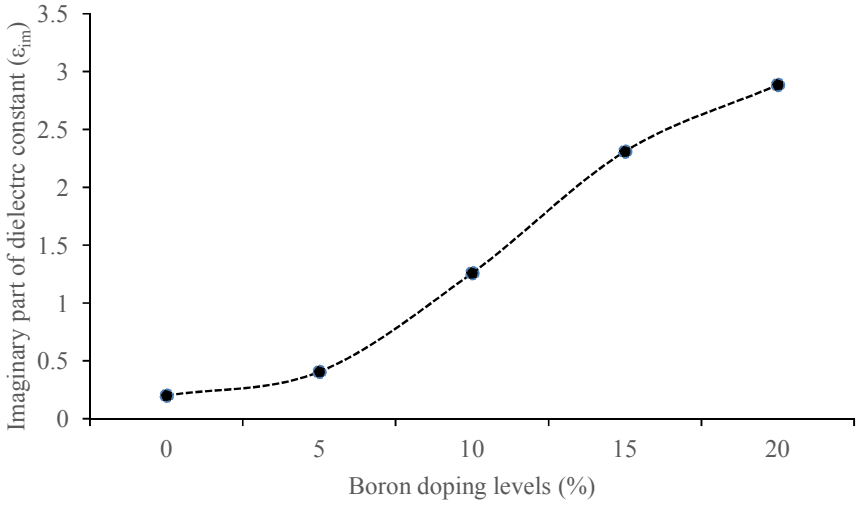

Fig. 11. Variation of imaginary part of dielectric constant of pure TiO_2 and B-TiO_2 thin films at 0, 5, 10, 15, and 20% concentrations

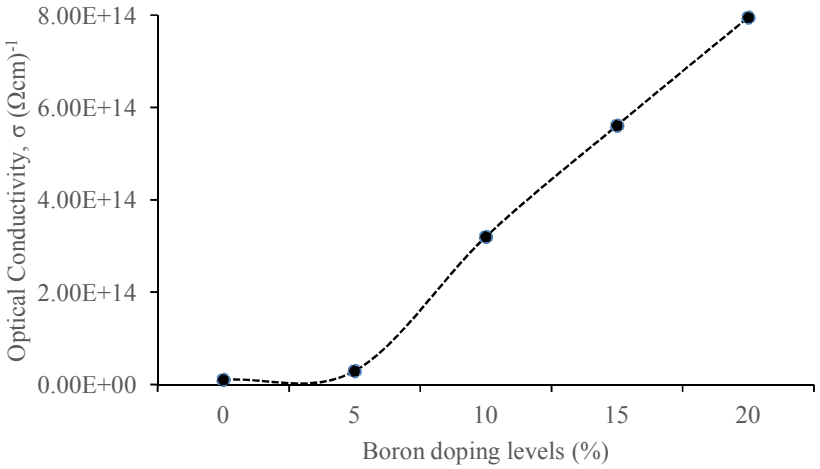

Fig. 12. Variation of optical conductivity for the pure TiO_2 and B-TiO_2 thin films

Figs 10 and 11 clearly revealed that both the real and imaginary parts of the dielectric constant increase with increase in boron doping concentration. The imaginary part increases slowly as the B concentration increases, whereas the real part of the dielectric constant increases sharply with increase in boron concentration, which shows that the loss factor of the thin films increases with increase in B doping concentration.

3.6 Optical Conductivity

The variations of optical conductivity of the films with concentration was determined from four-point probe measurement as illustrated in Fig. 12.

The above results shows that the optical conductivity increases with the increase in boron doping concentration and this might be due to the increase in absorption coefficient. The influence from grain boundary scattering decreases as the boron addition increases, but at 0% the crystallite size is small and the grain boundary scattering is dominant, which limits the film conductivity. The low free electron density of the undoped TiO_2 film makes the conductivity close to zero. As boron doping concentrations increased above (B / [B+Ti]) = 5%, the optical conductivity of the thin films increases rapidly with 20% having the highest optical conductivity due to the increase in free electron density.

4. CONCLUSION

The optical properties, electrical properties and microstructural images of undoped TiO_2, 5, 10, 15, and 20% B-TiO_2 thin films prepared by the sol-gel technique using spin coating method were investigated in this present study. The microstructural analysis revealed that (B / [B+Ti]) = 10% is the tolerable amount of boron doping concentration into the TiO_2 for achieving spherical shaped materials with low agglomeration, indicating that the thin films have a uniform, well disperse particles and high surface area. The obtained results illustrated that all the thin films deposited have high optical transmittance values in the range of 90-96% in the visible spectra region but with minimum transmittance of 52% observed for the pure TiO_2 thin films. This shows that the values of transmittance are high in the visible and near-infrared region and it is minimum in the ultraviolet region. The value of the optical band gap energy are desirably wide and range from 3.38eV to about 3.35eV, 3.28eV, 3.26eV, and it reached 3.36eV for (B / [B+Ti]) = 0, 5, 10, 15, and 20% boron doping concentration. The absorption threshold shifted in the wavelength range from about 320 nm to 380 nm and absorption peaks are found in the ultraviolet region near the wavelength 330 nm but very low at the visible and infrared regions of solar spectra because of higher transmittance of the thin films in this region. The shifting of the anatase peak and the phase change was due to the doping concentration of the boron to TiO_2, lead to decreased anatase crystal, particle sizes, and increased pore volume and surface area. The refractive index increases from 1.910 to 1.922 as B doping concentrations increases above 10%, and drastically decreased to 1.891. The imaginary part of the dielectric constant increase

slowly, whereas the real part increases sharply and the optical conductivity was found to increase with the increase in boron addition and this might be due to the increase in absorption coefficient. The present work shows that by controlling the particle size, it is possible to attain almost 99% transmission in the visible range. The achieved parameters are critical for developing photovoltaic cells and other optoelectronic applications.

ACKNOWLEDGMENTS

Authors appreciate University of Abuja, Nigeria for the partial financial support and the Laboratory staff of the Physics Advanced Laboratory, Sheda Science and Technology Complex (SHESTCO), Abuja, Nigeria for synthesis and characterization of the samples.

COMPETING INTERESTS

Authors have declared that no competing interests exist.

REFERENCES

1. Aljufairi NH. Electric properties and surface structure of TiO_2 for solar cells. Energy. 2012;39:6-10.
2. Dislich H. Sol-gel technology for thin films, In: Klein L. (Ed.), Noyes, Park Ridge: NJ. 1988;67.
3. Verma A, Kar M, Agnihotry SA. Aging effect of diethnolamine stabilized sol on different properties of TiO_2 films: Electrochromic applications. Solar Energy Materials and Solar Cells. 2007;91:1305-1312.
4. Zhang W, Yang B, Chen J. Effects of calcination temperature on preparation of boron-doped TiO_2 by sol-gel method. International Journal of Photoenergy. 2012;528637:1-8. Availlable:http://doi.org/10.1155/2012/528637
5. Mulmi DD, Thapa D, Dahal B, Baral D, Solanki PR. Spectroscopic studies of boron doped titanium dioxide nano-particles. International Journal of Materials Science and Engineering. 2016;4(3):172-178. Availlable:http://doi.org/10.17706/ijmse.2016.4.3
6. Bedikyan L, Zakhariev S, Zakharieva M. Titanium dioxide thin films: Preparation and optical properties. Journal of Chemical Technology and Metallurgy. 2013;48(6): 555-558.
7. Zhang WF, Zhang MS, Yin Z, Chen Q. Photoluminescence in anatase titanium dioxide nanocrystals. Appl. Phys. B: Lasers Opt. 2000;70:261-265.
8. Etacheri V, Valentin CD, Schneider J, Bahnemann D, Pillai SC. Visible-Light Activation of TiO_2 photocatalysts: Advances in theory and experiments. J. Photochem. and Photobiol. C: Photochem. Reviews. 2015;25:1-29. DOI: 10.1016/j.jphotochemrev.2015.08.003
9. Vorontsov AV, Stoyanova IV, Kozlov DV, Simagina VI, Savinov EN. Kinetics of the photocatalytic oxidation of gaseous acetone over platinized titanium dioxide. J. Catal. 2000;189:360-369.
10. Ni M, Leung MK, Leung DY, Sumathy K. A review and recent developments in photocatalytic water-splitting using TiO_2 for hydrogen production. Renewable and Sustainable Energy Reviews. 2007;11: 401-425.
11. Devi LG, Kavitha R. A review on non metal ion doped titania for the photocatalytic degradation of organic pollutants under UV/solar light: Role of photogenerated charge carrier dynamics in enhancing the activity. Appl. Catal. B. 2013;140-141:559-587.
12. Gómez M, Rodríguez J, Lindquist SE, Granqvist CG. Photoelectrochemical studies of dye-sensitized polycrystalline titanium oxide thin films prepared by sputtering. Thin solid films. 1999;342:148-152.
13. Ansón-Casaos A, Sampaio MJ, Jarauta-Córdoba J, Martínez MT, Silva CG, Faria JL, Silva AM. Evaluation of sol-gel TiO_2 photocatalysts modified with carbon or boroncompounds and crystallized in nitrogen or air atmospheres. Chemical Engineering Journal. 2015;277:11-20.
14. Zhu J, Chen F, Zhang J, Chen H, Anpo M. Fe^{3+}-TiO_2 Photocatalysts Prepared by combining sol-gel method with hydro-thermal treatment and their characterization. J. Photochem. Photobiol. A 2006;180: 196-204.
15. Zhang L, Tan PY, Lim CK, Guo X, Tse MS, Tan OK, Chang VWC. N-TiO_2-coated polyester filters for visible light-Photocatalytic removal of gaseous toluene under static and dynamic flow conditions. J. Environ. Chem. Eng. 2016;4(1):357-364.

Availlable:http://dx.doi.org/10.1016/j.jece.2015.11.027.

16. Grabowska E, Zaleska A, Sobczak JW, Gazdac M, Hupka J. Boron-doped TiO_2: Characteristics and photoactivity under visible light. Procedia Chemistry. 2009;1: 1553-1559.
17. Wang WK, Chen JJ, Gao M, Huang YX, Zhang X, Yu HQ. Photocatalytic degradation of atrazine by boron-doped TiO_2 with a tunable rutile/anatase ratio. Appl. Catal. B. 2016;195:69-76.
18. Yang K, Dai Y, Huang B. Origin of the photoactivity in boron-doped anatase and rutile TiO_2 calculated from first principles. Phys. Rev. B: Condens. Matter Mater. Phys. 2007;76:195201.
19. Zaleska A, Grabowska E, Sobczak JW, Gazdac M, Hupka J. Photocatalytic activity of boron-modified TiO_2 under visible light: The effect of boron content, calcination temperature and TiO_2 Matrix. Appl. Catal. B. 2009;89:469-475.
20. Zhao W, Ma WH, Chen CH, Zhao JC, Shuai ZG. Efficient degradation of toxic organic pollutants with Ni_2O_3/TiO_2-xBx under visible irradiation. Journal of the American Chemical Society. 2004;126(15): 4782-4783.
21. Diana VW, Qing CX, Mahasin AS, Kok HL, Tuti ML, Timothy TYT. Experimental and theoretical studies of Fe-doped TiO_2 films prepared by peroxo sol-gel method. Applied Catalysis A: General. 2011;401: 98-105.
22. Zaleska A, Sobczak JW, Grabowska E, Hupka J. Preparation and photocatalytic activity of boron-modified TiO_2 under UV and visible light. Appl. Catal. B. 2008;78: 92-100.
23. Quiñones DH, Rey A, Álvarez PM, Beltrán FJ, Puma GL. Boron doped TiO_2 catalysts for photocatalytic ozonation of aqueous mixtures of common pesticides: Diuron, o-phenylphenol, MCPA and terbuthylazine. Appl. Catal. B-Environmental. 2015;178: 74-81.
24. Sönmezoglu S, Erdogan BA. Investigation of optical, structural and morphological properties of nanostructured boron doped TiO_2 thin films. Bulletin of Materials Science. 2013;36(7):1239-1245.
25. Goswami A. Thin film fundamentals. New Age International Ltd. Publishers, New Delhi; 2005.
26. Rajashree C, Balu AR, Nagarethinam VS. Substrate temperature effect on the physical properties of spray deposited Lead sulfide thin films suitable for solar control coatings. International Journal of Chem. Tech. Research. 2014;6:347-360.
27. Forouhi AR, Bloomer I. Optical properties of crystalline semiconductors and dielectrics. Phys. Rev. B. 1988;38(3):1865. Availlable:https://doi.org/10.1103/PhysRevB.38.1865
28. Tanemura S, Miao L, Jin P, Kaneko K, Terai AN, Nabatova-Gabain N. Optical properties of polycrystalline and epitaxial anatase and rustile TiO_2 thin films by rf magnetron sputtering. Applied Surface Science. 2003;212-213:654-660.
29. Tauc J, Grigorovici R, Vancu A. Optical properties and electronic structure of amorphous germanium. Phys. Status Solidi. 1966;15:627-637.
30. Klan MI, Bhati KA, Qindeel R, Alonizan N, Althobaiti HS. Characterizations of multilayer ZnO thin films deposited by sol-gel spin coating technique. Results in Physics. 2017;7:651-655. Availlable:https://doi.org/10.1016/j.rinp.2016.12.029
31. Mezhenny S, Maksymovych P, Thompson TL. STM studies of defect production on the TiO_2(110)-(1X1) and TiO_2(110)-(1X2) surfaces induced by UV irradiation. Chemical Physics Letters. 2003;369:152-158.
32. Daimei C, Dong Y, Qun W, Zhongyi J. Effects of boron doping on photocatalytic activity and microstructure of titanium dioxide nanoparticles. Ind. Eng. Chem. Res. 2006;45:4110-4116.
33. Wu Y, Xing M, Zhang J, Chen F. Effective visible light-active boron and carbon modified TiO_2 photocatalyst for degradation of organic pollutant. Appl. Catal. B Environ. 2010;97:182-189.
34. Carmichael P, Hazafy D, Bhachu DS, Mills A, Darr JA, Parkin IP. Atmospheric pressure chemical vapor deposition of boron doped titanium dioxide for photocatalytic water reduction and oxidation. Phys. Chem. Chem. Phys. 2013; 15:16788-16794.
35. Hagiwara Y, Nakada T, Kunioka A. Improved J (sc) in CIGS thin film solar cells using a transparent conducting ZnO:B window layer. Solar Energy Materials and Solar Cells. 2001;67(1-4):267-271.
36. Cavalcante RP, Dantas RF, Bayarri B, González O, Giménez J, Esplugas S, Machulek Jr A. Synthesis and

characterization of B-doped TiO2 and their performance for the degradation of metoprolol. Catal. Today. 2015;252:27-34.
37. Quesada-González M, Boscher ND, Carmalt CJ, Parkin IP. Interstitial boron-doped TiO_2 thin films: The significant effect of boron on TiO_2 coatings grown by Atmospheric Pressure Chemical Vapor Deposition. ACS Appl. Mater. Interfaces. 2016;8:25024-25029.
38. Singh P, Kumar A, Kaur D. Mn-doped ZnO nanocrystalline thin films prepared by ultrasonic spray pyrolysis. Journal of Alloys and Compounds. 2009;471:11-15.
39. Begum NS, Ahmed HM, Hussain OM. Characterization and photocatalytic activity of boron-doped TiO_2 thin films prepared by liquid phase deposition technique. Bulletin Material Sciece. 2008; 31(5):741-745.
40. Ribalski MW. Handbook of optical constants of solids I. Academic Press, San Diego; 1998.

Peer-review history:
The peer review history for this paper can be accessed here:
http://www.sciencedomain.org/review-history/26664